

Influence of intraspecies interactions on the diversity of the wetting phase diagram in dilute ternary Bose-Einstein condensates

Nguyen Van Thu

Department of Physics, Hanoi Pedagogical University 2, Hanoi, 100000, Vietnam

Abstract

We investigate the influence of intraspecies interactions on the structure and diversity of the wetting phase diagram in a dilute ternary Bose-Einstein condensates. Within the GP formalism, we employ the double-parabola approximation to describe the interfacial properties of the system in the limit of strong segregation between two of the components. Our analysis focuses on the static behavior near degenerate points where distinct phase boundaries intersect in the parameter space defined by the healing-length ratios. We demonstrate that the first-order and critical wetting transition lines, along with the nucleation line intersect at a unique degenerate point. This finding contrasts with previous studies in the interspecies interaction space, where two degenerate points were observed. These results provide new insights into the interfacial phase behavior of multicomponent quantum gases and offer theoretical guidance for experimental explorations of wetting phenomena in ultracold atomic systems.

Keywords: Ternary Bose-Einstein condensates, Wetting phase diagram, Degenerate points

1. Introduction

The wetting phenomenon is a well-known and widely observed occurrence in both natural and everyday contexts [1, 2]. In classical fluid systems, wettability is typically analyzed in terms of intermolecular interactions. In the context of quantum physics, the wetting phenomenon was first described in type-I superconducting materials, as introduced by Landau and Ginzburg in

1950 [3]. Within the framework of mean-field theory for critical phenomena, the wetting phase transition in superconductors is interpreted as the delocalization or unbinding of the interface between the normal and superconducting phases in type-I superconductors [4]. This wetting phase transition has been experimentally observed in conventional superconductors [5] and has also been reported in high-temperature superconducting materials [6]. Furthermore, the phenomenon of wetting phase transitions has been extensively studied in magnetic systems [7].

The wetting phenomenon in Bose-Einstein condensates (BECs) was first predicted theoretically in 2004 [8], in the context of a two-component BEC confined by an idealized hard-wall (optical wall). Despite the theoretical interest it has garnered, this phenomenon has yet to be observed experimentally, even after more than two decades. Several hypotheses have been advanced to explain this absence, accompanied by a range of theoretical and experimental efforts aimed at overcoming the associated challenges. One key limitation is the ideal nature of the hard-wall potential, which cannot be realized in practical experimental setups. To address this issue, alternative approaches have been proposed, including the replacement of the hard-wall confinement with a more experimentally accessible soft-wall potential [9], and investigations into the thermodynamic behavior of the prewetting transition [10].

A more recent development involves the substitution of the conventional hard- or soft-wall boundary by a third constituent within a ternary (three-component) BECs system [11]. This configuration is characterized not only by the atomic masses m_i , ($i = 1, 2, 3$), but also by six intrinsic interaction parameters: three intraspecies scattering lengths a_{ii} , and three interspecies scattering lengths $a_{ij} = a_{ji}$, ($i, j = 1, 2, 3, i \neq j$). Additionally, the system comprises three independent particle densities n_i . The presence of a third component in BEC systems markedly increases the number of experimentally controllable parameters, particularly the relative coupling constants K_{13} , K_{23} and the healing length ratios ξ_i/ξ_j (see below). These parameters can be tuned either independently or in conjunction, in BEC mixtures composed of two hyperfine states of a single atomic species or of two distinct atomic species [12, 13, 14, 15, 16]. A notable example involves laser-induced shifts of magnetic Feshbach resonances in ^{87}Rb , which permit precise tuning of the scattering lengths while maintaining significantly lower particle loss rates than those associated with optical Feshbach resonances [14]. Furthermore, multicomponent systems featuring both ferromagnetic and antiferromagnetic

spin–spin interactions offer an extended degree of control [16]. In mixtures of ^{87}Rb and ^{133}Cs , the interspecies scattering length—which characterizes atomic interactions—has been successfully manipulated using magnetic Feshbach resonances in magnetic quadrupole traps, followed by confinement in levitated optical traps [12], or through the use of cigar-shaped trapping geometries [13]. This enhanced tunability gives rise to increasingly rich and intricate wetting phase diagrams, underscoring the complexity and flexibility of multicomponent BEC systems.

In Ref. [11], the wetting phase diagram was systematically analyzed within the parameter space spanned by the interspecies interaction coupling constants, while the intraspecies interaction strengths were held fixed. Phase diagrams were constructed for both symmetric and asymmetric configurations, revealing the existence of degenerate points. Both first-order and critical wetting transitions were identified within these regimes. As the remaining focus of this work, we investigate the wetting phase diagram of a dilute ternary BEC in the parameter space defined by the ratios of healing lengths. These ratios are experimentally tunable by varying the intraspecies atomic interaction strengths while keeping the interspecies interactions fixed.

The paper is organized as follows: Section 2 we have a brief the DPA for the wave functions of a ternary BEC in strong segregation limit between components 1 and 2. The wetting phase diagram and loci of degenerate points are investigated in Section 3. Conclusions are reported in Section 4.

2. Wave functions of a dilute ternary BEC in double parabola approximation

In this Section we summarize the results for wave functions in DPA presented in Ref. [11]. We start by considering a dilute ternary BEC consisting of three components confined within a volume V in the absence of external fields. Within the framework of the grand canonical ensemble, the thermodynamic properties of the system are governed by the grand potential functional

$$\Omega = \int_V d^3\vec{r} \left\{ \sum_{i=1}^3 \left[-\frac{\hbar^2}{2m_i} \psi_i^*(\vec{r}) \nabla^2 \psi_i(\vec{r}) \right] + V_{\text{GP}} \right\}, \quad (1)$$

in which Gross-Pitaevskii (GP) potential is

$$V_{\text{GP}} = \sum_{i=1}^3 \left[-\mu_i |\psi_i(\vec{r})|^2 + \frac{G_{ii}}{2} |\psi_i(\vec{r})|^4 \right] + \sum_{i < j} G_{ij} |\psi_i(\vec{r})|^2 |\psi_j(\vec{r})|^2. \quad (2)$$

Here \hbar denotes the reduced Planck constant, μ_i is the chemical potential of the i -th component, and $\psi_i(\vec{r})$ is the macroscopic wave function associated with that component. In the absence of superfluid flow, the wave functions can be taken as real and serve as order parameters. The local condensate density of each component is then defined by $n_i(\vec{r}) \equiv |\psi_i(\vec{r})|^2$. The interaction strengths are characterized by the coupling constants. In the dilute BECs, where the s -wave scattering lengths a_{ii} and a_{ij} are much smaller than the average interatomic spacing, the interatomic interactions can be modeled as contact potentials. In this limit, the intraspecies coupling constants take the form

$$G_{ii} = \frac{4\pi\hbar^2 a_{ii}}{m_i}, \quad (3)$$

while the interspecies coupling constants are given by

$$G_{ij} = 2\pi\hbar^2 \left(\frac{1}{m_i} + \frac{1}{m_j} \right) a_{ij}, \quad (4)$$

For convenience, we introduce the dimensionless interspecies coupling parameters

$$K_{ij} \equiv \frac{G_{ij}}{\sqrt{G_{ii}G_{jj}}} = \frac{m_i + m_j}{2\sqrt{m_i + m_j}} \frac{a_{ij}}{\sqrt{a_{ii}a_{jj}}}. \quad (5)$$

which quantify the relative strength of interspecies interactions. In this work, we restrict our attention to the immiscible regime, characterized by $K_{ij} > 1$. For each component, the characteristic length is the healing length, which is defined as $\xi_j \equiv \hbar/\sqrt{2m_i\mu_i} = \hbar/\sqrt{2m_jG_{ii}n_i}$. Therefore, the healing length ratio depends on atomic parameter [9, 11]

$$\frac{\xi_i}{\xi_j} = \left(\frac{n_j a_{jj}}{n_i a_{ii}} \right)^{1/2} = \left(\frac{m_j a_{jj}}{m_i a_{ii}} \right)^{1/4}. \quad (6)$$

We now proceed to describe the system under consideration. The system exhibits translational symmetry in the (x, y) -plane and is inhomogeneous

along the z -axis. At the initial time, two condensates, labeled as components 1 and 2, are in two-phase equilibrium, and a stable interface between them, referred to as the 1–2 interface, is present. This implies that the bulk pressures of the two condensates are equal $P_1 = P_2 \equiv P$, where the bulk pressure P_i of component i is given by

$$P_i = \frac{\mu_i^2}{2G_{ii}}. \quad (7)$$

Condensate 1 occupies the bulk region at $z \rightarrow -\infty$ while condensate 2 occupies the bulk region at $z \rightarrow \infty$. Subsequently, a third component (condensate 3) is introduced at the 1–2 interface and is considered a candidate for the wetting phase. For convenience, we define the auxiliary chemical potential $\bar{\mu}_3$, the auxiliary condensate density \bar{n}_3 and the auxiliary healing length $\bar{\xi}_3$, which satisfy the following relations

$$\begin{aligned} \bar{\mu}_3 &= \sqrt{\frac{G_{33}}{G_{11}}}\mu_1 = \sqrt{\frac{G_{33}}{G_{22}}}\mu_2, \\ \bar{n}_3 &= \frac{\bar{\mu}_3}{G_{33}}, \\ \bar{\xi}_3 &= \frac{\hbar}{\sqrt{2m_3\bar{\mu}_3}}. \end{aligned} \quad (8)$$

It is evident from these definitions that $\mu_3 \leq \bar{\mu}_3$ and $n_3 \leq \bar{n}_3$. Under this configuration, the boundary conditions for the condensate wavefunctions in the bulk are given by

$$\begin{aligned} \psi_1(-\infty) &= \sqrt{n_1}, \quad \psi_2(\infty) = \sqrt{n_2}, \\ \psi_1(\infty) &= \psi_2(-\infty) = \psi_3(\infty) = \psi_3(-\infty) = 0. \end{aligned} \quad (9)$$

By performing rescalings analogous to those introduced in Ref. [11], namely, $\psi_1 = \sqrt{n_1}\tilde{\psi}_1$, $\psi_2 = \sqrt{n_2}\tilde{\psi}_2$, $\psi_3 = \sqrt{n_3}\tilde{\psi}_3$ and $z = \xi_2\tilde{z}$ one obtains a set of three coupled GP equations, as detailed in Ref. [11]

$$\begin{aligned} \left(\frac{\xi_1}{\xi_2}\right)^2 \frac{d^2\tilde{\psi}_1}{d\tilde{z}^2} &= -\tilde{\psi}_1 + \tilde{\psi}_1^3 + \sum_{j \neq 1} K_{1j} \tilde{\psi}_j^2 \tilde{\psi}_1, \\ \frac{d^2\tilde{\psi}_2}{d\tilde{z}^2} &= -\tilde{\psi}_2 + \tilde{\psi}_2^3 + \sum_{j \neq 2} K_{2j} \tilde{\psi}_j^2 \tilde{\psi}_2, \\ \left(\frac{\bar{\xi}_3}{\xi_2}\right)^2 \frac{d^2\tilde{\psi}_3}{d\tilde{z}^2} &= -\frac{\mu_3}{\bar{\mu}_3} \tilde{\psi}_3 + \tilde{\psi}_3^3 + \sum_{j \neq 3} K_{3j} \tilde{\psi}_j^2 \tilde{\psi}_3. \end{aligned} \quad (10)$$

The boundary conditions (9) reduce

$$\begin{aligned}\tilde{\psi}_1(-\infty) &= 1, \quad \tilde{\psi}_2(\infty) = 1, \\ \tilde{\psi}_1(\infty) &= \tilde{\psi}_2(-\infty) = \tilde{\psi}_3(\infty) = \tilde{\psi}_3(-\infty) = 0.\end{aligned}\quad (11)$$

In the remainder of this work, we focus on the regime in which components 1 and 2 are in the strong segregation limit, characterized by $K_{12} \rightarrow \infty$ as treated within the framework of the DPA introduced in Ref. [17]. We choose the coordinate origin $\tilde{z} = 0$ to coincide with the interface between condensates 1 and 2. Under this limit, the system is naturally partitioned into three spatial domains. Domain I, defined by $\tilde{z} \in (-\infty, \tilde{z}^-]$, comprises condensates 1 and 3, whose density profiles intersect at a point $\tilde{z} = \tilde{z}^-$. In this region, the GP potential (2) is expanded to second order in deviations from the bulk density of component 1 (i.e., $\tilde{\psi}_1 = 1$) and around zero for component 3. The resulting DPA potential in domain I takes the form

$$\tilde{V}_I^{(DPA)} = -2(1 - \tilde{\psi}_1)^2 - \left(K_{13} - \frac{\mu_3}{\bar{\mu}_3} \right) \tilde{\psi}_3^2. \quad (12)$$

Here we use $\tilde{V} = V/(g_{11}n_1^2/2)$, which is dimensionless potential. From (12) the coupled GP equations in (10) become

$$\begin{aligned}\left(\frac{\xi_1}{\xi_2}\right)^2 \tilde{\psi}_1'' &= -2(1 - \tilde{\psi}_1), \\ \left(\frac{\bar{\xi}_3}{\xi_2}\right)^2 \tilde{\psi}_3'' &= \left(K_{13} - \frac{\mu_3}{\bar{\mu}_3} \right) \tilde{\psi}_3^2.\end{aligned}\quad (13)$$

The general solutions to Eq. (13), subject to the boundary conditions specified in Eq. (11), are given by

$$\tilde{\psi}_1 = 1 - A_1 e^{\frac{\xi_2}{\xi_1} \tilde{z}}, \quad \tilde{\psi}_2 = 0, \quad \tilde{\psi}_3 = A_3 e^{\sqrt{K_{13} - \frac{\mu_3}{\bar{\mu}_3}} \frac{\xi_2}{\xi_3} \tilde{z}}. \quad (14)$$

Domain III, defined by $\tilde{z} \in [\tilde{z}^+, \infty)$, contains condensates 2 and 3, which intersect at $\tilde{z} = \tilde{z}^+$. By symmetry with domain I, the DPA potential corresponding solutions in domain III is

$$\tilde{V}_{III}^{(DPA)} = -2(1 - \tilde{\psi}_2)^2 - \left(K_{23} - \frac{\mu_3}{\bar{\mu}_3} \right) \tilde{\psi}_3^2, \quad (15)$$

therefore the wave functions for the condensates are

$$\tilde{\psi}_1 = 0, \quad \tilde{\psi}_2 = 1 - D_2 e^{-\sqrt{2}\tilde{z}}, \quad \tilde{\psi}_3 = D_3 e^{-\sqrt{K_{23} - \frac{\mu_3}{\bar{\mu}_3} \xi_3} \tilde{z}}. \quad (16)$$

Domain II, defined by $\tilde{z} \in [\tilde{z}^-, \tilde{z}^+]$ serves as the intermediate region, in which condensates 1 and 3 coexist for $\tilde{z} \in [\tilde{z}^-, 0]$ and condensates 2 and 3 coexist for $\tilde{z} \in [0, \tilde{z}^+]$. In this domain, the wave function of condensate 3 varies from its maximum value $\sqrt{\mu_3/\bar{\mu}_3}$ whereas the deviation of wave functions for condensates 1 and 2 are small from zero. The DPA potential reads

$$\begin{aligned} \tilde{V}_{\text{II}}^{(\text{DPA})} = & -\frac{1}{2} + \frac{1}{2} \left(\frac{\mu_3}{\bar{\mu}_3} \right)^2 - 2 \frac{\mu_3}{\bar{\mu}_3} \left(\sqrt{\frac{\mu_3}{\bar{\mu}_3}} - \tilde{\psi}_3 \right)^2 \\ & - \left(\frac{\mu_3}{\bar{\mu}_3} K_{13} - 1 \right) \tilde{\psi}_1^2 - \left(\frac{\mu_3}{\bar{\mu}_3} K_{23} - 1 \right) \tilde{\psi}_2^2. \end{aligned} \quad (17)$$

The condensate wavefunctions in this region take the form

$$\begin{aligned} \tilde{\psi}_1 &= 2B_1 \sinh(\sqrt{\frac{\mu_3}{\bar{\mu}_3} K_{13} - 1} \frac{\xi_2}{\xi_1} \tilde{z}), \quad \text{for } \tilde{z} < 0, \\ \tilde{\psi}_2 &= -2C_2 \sinh(\sqrt{\frac{\mu_3}{\bar{\mu}_3} K_{23} - 1} \tilde{z}), \quad \text{for } \tilde{z} > 0, \\ \tilde{\psi}_3 &= \sqrt{\frac{\mu_3}{\bar{\mu}_3}} + B_3 \exp(\sqrt{2} \sqrt{\frac{\mu_3}{\bar{\mu}_3} \frac{\xi_2}{\xi_3}} \tilde{z}) + C_3 \exp(-\sqrt{2} \sqrt{\frac{\mu_3}{\bar{\mu}_3} \frac{\xi_2}{\xi_3}} \tilde{z}). \end{aligned} \quad (18)$$

The general solutions in Eqs. (33), (16) and (34) contain eight integration constants $A_1, A_3, B_1, B_3, C_2, C_3, D_2, D_3$. These constants are determined by enforcing continuity of the condensate wave functions and their first derivatives. Specifically, continuity conditions for $\tilde{\psi}_1, \tilde{\psi}_3$ are imposed at \tilde{z}^- while those for $\tilde{\psi}_2, \tilde{\psi}_3$ are imposed at \tilde{z}^+ ,

$$\begin{aligned} \tilde{\psi}_1(\tilde{z} \rightarrow \tilde{z}^- + 0) &= \tilde{\psi}_1(\tilde{z} \rightarrow \tilde{z}^- - 0), \quad \tilde{\psi}_3(\tilde{z} \rightarrow \tilde{z}^- + 0) = \tilde{\psi}_3(\tilde{z} \rightarrow \tilde{z}^- - 0), \\ \tilde{\psi}_2(\tilde{z} \rightarrow \tilde{z}^+ + 0) &= \tilde{\psi}_2(\tilde{z} \rightarrow \tilde{z}^+ - 0), \quad \tilde{\psi}_3(\tilde{z} \rightarrow \tilde{z}^+ + 0) = \tilde{\psi}_3(\tilde{z} \rightarrow \tilde{z}^+ - 0), \\ \tilde{\psi}'_1(\tilde{z} \rightarrow \tilde{z}^- + 0) &= \tilde{\psi}'_1(\tilde{z} \rightarrow \tilde{z}^- - 0), \quad \tilde{\psi}'_3(\tilde{z} \rightarrow \tilde{z}^- + 0) = \tilde{\psi}'_3(\tilde{z} \rightarrow \tilde{z}^- - 0), \\ \tilde{\psi}'_2(\tilde{z} \rightarrow \tilde{z}^+ + 0) &= \tilde{\psi}'_2(\tilde{z} \rightarrow \tilde{z}^+ - 0), \quad \tilde{\psi}'_3(\tilde{z} \rightarrow \tilde{z}^+ + 0) = \tilde{\psi}'_3(\tilde{z} \rightarrow \tilde{z}^+ - 0). \end{aligned} \quad (19)$$

Although this procedure yields a complete system of eight equations, the resulting expressions are algebraically lengthy and do not yield additional physical insight. For this reason, we omit their explicit forms here.

3. Wetting phase diagram and loci of degenerate points

3.1. Wetting phase diagram

In this section, we examine the wetting phase transition and derive the corresponding wetting phase diagram. To this end, we begin by recalling some results previously reported in Ref. [11]. As discussed in the preceding section, we initially consider a system comprising two components, labeled 1 and 2, which coexist in a two-phase equilibrium. Under these conditions, the interface between components 1 and 2 represents a stable configuration. Subsequently, component 3 is introduced at the 1-2 interface. This third component acts as a surfactant under the condition

$$P_3 = \left(\frac{\mu_3}{\bar{\mu}_3} \right)^2 P \leq P_1 = P_2 = P. \quad (20)$$

As a result, three distinct interfaces are formed: 1-3, 2-3, and the original 1-2 interface, now modified by the presence of the surfactant. When the surfactant is formed, a nucleation is created with a small thickness layer. The condition for the nucleation is found

$$\sqrt{2} \left(\frac{\xi_1}{\bar{\xi}_3} + \frac{\xi_2}{\bar{\xi}_3} \right) \left(\frac{\mu_3}{\bar{\mu}_3} \right)^{3/2} = \sqrt{K_{13} - \frac{\mu_3}{\bar{\mu}_3}} + \sqrt{K_{23} - \frac{\mu_3}{\bar{\mu}_3}}. \quad (21)$$

The interfacial tension at the interface 1-2 with presence of the surfactant is defined as

$$\gamma_{12(3)} \equiv 4P \xi_2 \int_{-\infty}^{\infty} d\tilde{z} \left[\left(\frac{\xi_1}{\xi_2} \frac{d\tilde{\psi}_1}{d\tilde{z}} \right)^2 + \left(\frac{d\tilde{\psi}_2}{d\tilde{z}} \right)^2 + \left(\frac{\bar{\xi}_3}{\xi_2} \frac{d\tilde{\psi}_3}{d\tilde{z}} \right)^2 \right]. \quad (22)$$

From an interfacial thermodynamics perspective, partial wetting corresponds to a competition between the excess free energies associated with three pairwise interfaces. In this regime, the interfacial tensions satisfy Antonov's rule [18]

$$\gamma_{12(3)} < \gamma_{13} + \gamma_{23}, \quad (23)$$

indicating that the 1-2 interface is not completely “covered” by a microscopic film of component 3. The surfactant layer thickness is defined as $\tilde{L} = \tilde{z}^+ - \tilde{z}^-$. A continuous wetting scenario arises when \tilde{L} increases smoothly from

zero to a macroscopic (divergent) value as the system parameters are varied. Along such trajectories in parameter space, the system evolves from partial wetting to complete wetting, where the interfacial free-energy balance reaches equality,

$$\gamma_{12(3)} = \gamma_{13} + \gamma_{23}. \quad (24)$$

This condition eliminates the thermodynamic barrier to full adsorption of component 3 at the 1–2 interface, and the corresponding continuous transition is identified as a critical wetting phase transition. Within the GP mean-field framework, imposing the equalities $\tilde{\psi}_1 = \tilde{\psi}_3$ at \tilde{z}^- and $\tilde{\psi}_2 = \tilde{\psi}_3$ at \tilde{z}^+ yields the critical wetting boundary at three-phase coexistence, which obeys [11]

$$\frac{\xi_1}{\xi_3 \beta_{13}} + \frac{\xi_2}{\xi_3 \beta_{23}} = \sqrt{2}. \quad (25)$$

A second possible scenario corresponds to a first-order wetting phase transition. In this regime, the interface free-energy balance prevents the formation of a microscopic film of component 3 at the 1–2 interface, and the third condensate remains metastable or unstable. The interfacial tensions must then satisfy Young's law [18]

$$\gamma_{12} \leq \gamma_{13} + \gamma_{23}. \quad (26)$$

which is the thermodynamic condition ensuring that the 1–2 interface cannot be completely wet by a surfactant layer of component 3. In geometric terms, Young's law may be interpreted as the vanishing or reduction of the contact angle at the interface separating the three condensates, providing a microscopic analogue of the Young–Laplace relation in classical capillarity theory. As the system parameters are varied, a first-order wetting transition occurs when the inequality (26) becomes equality, eliminating the interfacial free-energy barrier and causing the film thickness to exhibit a discontinuous jump from zero to a finite value. This discontinuity distinguishes first-order wetting from the continuous (critical) scenario and reflects the metastability of the prewetting state near coexistence. At the two-phase coexistence regime, the interfacial tension in the absence of the surfactant is evaluated using the DPA [17] and is given by

$$\gamma_{ij}^{(\text{DPA})} = 2\sqrt{2} \frac{\beta_{ij}}{\sqrt{2} + \beta_{ij}} P(\xi_i + \xi_j), \quad (27)$$

where $\beta_{ij} = \sqrt{K_{ij} - 1}$. Substituting Eq. (27) into Eq. (26), we obtain the following relation

$$\frac{\xi_1}{\xi_3} + \frac{\xi_2}{\xi_3} = \frac{\beta_{13}}{\sqrt{2} + \beta_{13}} \left(1 + \frac{\xi_1}{\xi_3} \right) + \frac{\beta_{23}}{\sqrt{2} + \beta_{23}} \left(1 + \frac{\xi_2}{\xi_3} \right). \quad (28)$$

Equation (28) represents the condition for the occurrence of a strongly first-order wetting transition, as discussed in Ref.[11].

We now turn our attention to examining the conditions under which the interface between components 1 and 2 may become wetted by the third component. As outlined previously, the relative parameters defined in Eqs. (5) and (6) are determined by intrinsic atomic parameters, particularly the intra- and interspecies scattering lengths. These interatomic interactions are experimentally tunable across several orders of magnitude in strength via the application of Feshbach resonances [19, 20, 21]. In the phase space spanned by these parameters, the wetting phase diagram at three-phase coexistence ($\mu_3/\bar{\mu}_3 = 1$) is determined by three boundaries: the nucleation line given by Eq. (21), the critical and first-order wetting lines given by Eqs. (25) and (28), respectively. Our system contains four independent parameters, $K_{13}, K_{23}, \xi_3/\xi_1$ and ξ_3/ξ_2 . In Ref. [11], the intraspecies scattering lengths were held fixed so that the healing-length ratios defined in Eq. (6) remain constant, and the wetting phase transitions were investigated in the (K_{13}, K_{23}) -plane by varying the interspecies scattering lengths. Within this construction, the wetting phase diagram appears two degenerate points, which separate the phase diagram plane into three regions: one inner corresponds to the critical wetting phase transition and two outers correspond to the first-order wetting phase transition.

We now investigate how the wetting phase transition is affected by variations in the healing-length ratios. Here, the relative coupling constants K_{13} and K_{23} are fixed, while the healing length ratios are modulated by varying the intraspecies scattering lengths. In particular, we hold ξ_1, ξ_2 constant, and investigate the effects of varying ξ_3 . In Fig. 1, the nucleation line showing by the blue line is plotted in $(\bar{\xi}_3/\xi_1, \mu_3/\bar{\mu}_3)$ -plane at $K_{13} = 3, K_{23} = 2K_{13}$ and $\bar{\xi}_3/\xi_2 = 2\bar{\xi}_3/\xi_1$. The nucleation line intersect the three-phase coexistent line (black line) at $\bar{\xi}_3/\xi_1 = 0.581$. In the symmetric case where $K_{13} = K_{23}$ and $\bar{\xi}_3/\xi_2 = \bar{\xi}_3/\xi_1$ this point at $(\bar{\xi}_3/\xi_1 = 1, \mu_3/\bar{\mu}_3 = 1)$.

As mentioned above, the interesting wetting phase diagrams for the symmetric and asymmetric case were considered while the interspecies interaction strengths were varied. Here we investigate the wetting phase diagram

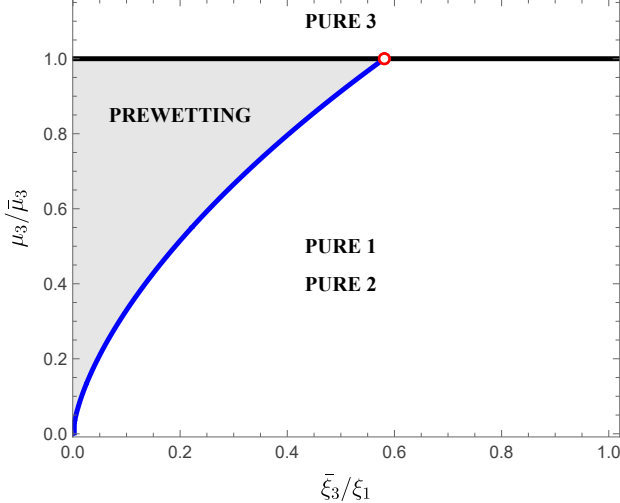


Figure 1: The nucleation line (blue line) of the surfactant as a function of $\bar{\xi}_3/\xi_1$ at $K_{13} = 3$, $K_{23} = 2K_{13}$ and $\bar{\xi}_3/\xi_2 = 2\bar{\xi}_3/\xi_1$.

in space of the intraspecies interaction strength. The wetting phase diagram at the three-phase coexistence is sketched in Fig. 2 at fixed $K_{13} = 3$ and $K_{23} = 2K_{13}$. The black, red and blue lines correspond to the nucleation line (21), critical wetting line (25) and first-order wetting line (28), respectively.

A remarkable distinction between the present results and those reported in Ref. [11] lies in the number of degenerate points observed. Specifically, in the current analysis, only a single degenerate point is identified, whereas Ref. [11] reported the existence of two degenerate points within the plane defined by the relative interspecies interaction coupling constants. This degenerate point corresponds to the condition at which the interfacial tensions satisfy an exact balance, namely, the equality (26), thereby marking the boundary between partial and complete wetting regions. Its uniqueness in the current parameter space implies a more constrained set of conditions under which the wetting transition occurs, reflecting the altered roles of the tunable parameters in this scenario. The reduction in the number of degenerate points highlights the sensitivity of the wetting behavior to the interplay between intra- and interspecies interactions, particularly under fixed relative coupling constants.

We now analyze the behavior of the interfacial tensions on either side of the degenerate point D in the wetting phase diagram. We begin with the

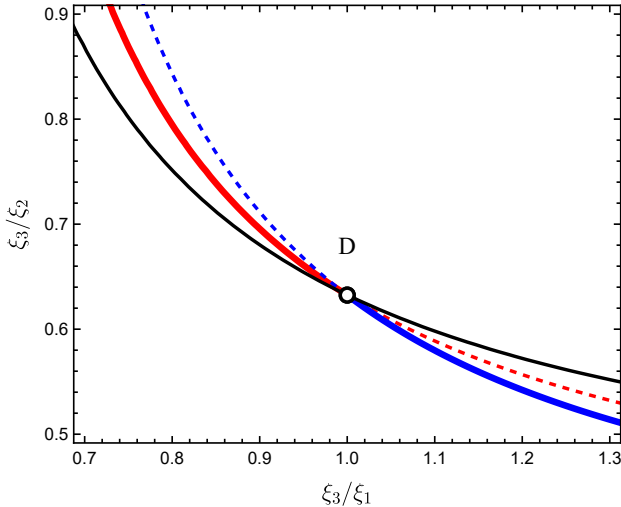


Figure 2: The wetting phase diagram in the $(\xi_3/\xi_1, \xi_3/\xi_2)$ -plane fixed $K_{13} = 3$ and $K_{23} = 2K_{13}$. The black line corresponds to the nucleation line, the red and blue lines correspond to the first-order and critical wetting lines.

region above point D. Using parameters similar to those employed in Fig. 2, we examine the variation of interfacial tensions along the path defined by $\frac{\xi_3}{\xi_1} = \frac{\xi_3}{\xi_2}$. The reduced interfacial tensions are presented in Fig. 3(a) as functions of the healing length ratio $\frac{\xi_3}{\xi_1} = \frac{\xi_3}{\xi_2}$ with fixed coupling constants $K_{13} = 3, K_{23} = 2K_{13}$. In this figure, the interfacial tensions $\gamma_{12}, \gamma_{13} + \gamma_{23}$ and the modified tension $\gamma_{12(3)}$ (i.e., the tension of the 1–2 interface in the presence of surfactant) are shown in black, red, and blue, respectively. The addition of the surfactant increases the interfacial tension of the 1–2 interface, resulting in $\gamma_{12(3)} > \gamma_{12}$. At point C the condition $\gamma_{12(3)} = \gamma_{13} + \gamma_{23}$ is satisfied, indicating the onset of wetting. As the healing length ratio $\frac{\xi_3}{\xi_1}$ decreases further $\gamma_{12(3)}$ also decreases but remains greater than both $\gamma_{13} + \gamma_{23}$ and γ_{12} . This behavior persists to the left of point W as well. Nevertheless, the minimum of the interfacial tensions is always given by $\gamma_{13} + \gamma_{23}$ confirming that this configuration is thermodynamically favorable in the wetting regime. As we follow the path $\frac{\xi_3}{\xi_1} = \frac{\xi_3}{\xi_2}$, the grand potential Ω exhibits a discontinuity in its first derivative at point W along the segment xWy. This discontinuity corresponds to a jump in the thickness of the surfactant layer from zero to a macroscopic value, signifying a strongly first-order wetting phase transition.

We now turn to the region below point D in the wetting phase diagram

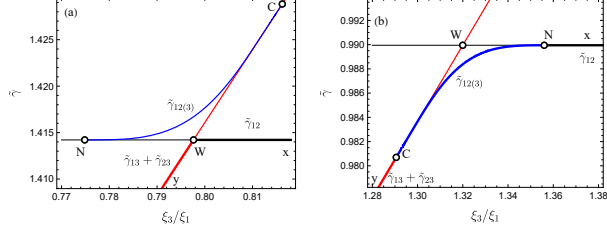


Figure 3: The reduced interfacial tension $\tilde{\gamma} = \gamma/(4P\xi_2)$ versus the healing length ratio ξ_3/ξ_1 at $K_{13} = 3$, $K_{23} = 2K_{13}$. The black, red and blue curves correspond to $\tilde{\gamma}_{12}$, $\tilde{\gamma}_{13} + \tilde{\gamma}_{23}$ and $\tilde{\gamma}_{12(3)}$, respectively; moving along a line (a) $\xi_3/\xi_2 = \xi_3/\xi_1$ and (b) $\xi_3/\xi_2 = 0.4\xi_3/\xi_1$.

of Fig. 2. In Fig. 3(b), we present the evolution of the interfacial tensions along the path defined by $\xi_3/\xi_2 = 0.4\xi_3/\xi_1$ again as a function of $\frac{\xi_3}{\xi_1}$. The color coding is consistent with Fig. 3(a). In this scenario, the behavior differs markedly from the previous case. At point N the surfactant is introduced at the 1–2 interface, and the interfacial tension $\gamma_{12(3)}$ begins to decrease, following the blue curve. At point C the condition $\gamma_{12(3)} = \gamma_{13} + \gamma_{23}$ is again satisfied. However, in this case, the slope of the grand potential Ω remains continuous as we move through point W along the path xNCy. Correspondingly, the thickness of the surfactant layer increases continuously from zero at point N to a macroscopic value at C. This smooth evolution indicates a continuous, or second-order (critical), wetting transition.

Now we consider at the degenerate point D. From (36) and (27) the results for the interfacial tensions are

$$\begin{aligned} \frac{\gamma_{12}}{4P\xi_2} &= \frac{1}{\sqrt{2}} \left(1 + \frac{\beta_{13}}{\beta_{23}} \right), \\ \frac{\gamma_{13}}{4P\xi_2} &= \frac{1}{\sqrt{2}} \frac{\beta_{13}}{\beta_{23}}, \\ \frac{\gamma_{23}}{4P\xi_2} &= \frac{1}{\sqrt{2}}. \end{aligned} \quad (29)$$

Eq. (29) shows that the Young law (26) is satisfied and the interfacial tensions are independent of the surfactant thickness layer. Furthermore, once Eq. (29) the interfacial tension $\gamma_{12(3)}$ is also independent of variables ξ_3/ξ_1 and ξ_3/ξ_2 .

In summary, the nature of the wetting transition depends sensitively on the location relative to the degenerate point D in the wetting phase diagram (Fig. 2). Specifically, the transition is of first order above point D, and is of

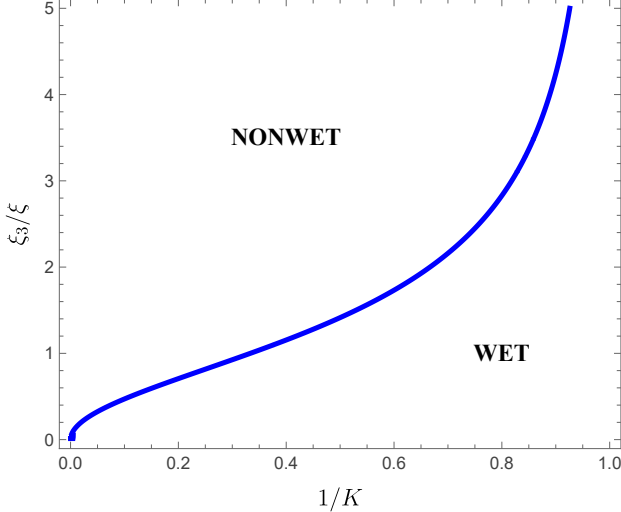


Figure 4: The wetting phase diagram in the complete symmetric system in $(1/K, \xi_3/\xi)$ -plane.

second order below it.

We consider the partial symmetric system, in which the interspecies coupling constants are the same, i.e., $K_{13} = K_{23} \equiv K$, equivalently, $\beta \equiv \beta_{13} = \beta_{23} = \sqrt{K - 1}$. The nucleation line (21) becomes

$$\left(\frac{1}{\xi_3/\xi_1} + \frac{1}{\xi_3/\xi_2} \right) \left(\frac{\mu_3}{\bar{\mu}_3} \right)^{3/2} = \sqrt{2}\beta. \quad (30)$$

At three-phase coexistence, the relations for nucleation line (30), first-order wetting (28) and critical wetting line (25) coincide and reduce to the following form

$$\frac{1}{\xi_3/\xi_1} + \frac{1}{\xi_3/\xi_2} = \sqrt{2}\beta. \quad (31)$$

This implies that the phase boundary line is degenerate. By repeating the analysis described in the previous subsections, we find that the wetting phase transition is of strongly first-order character. This is evidenced by a discontinuous jump in the thickness of the surfactant layer from zero to a macroscopic value at the transition point.

In case of the complete symmetry, i.e., $K_{13} = K_{23} \equiv K$ and $\xi_1 = \xi_2 \equiv \xi$, the nucleation, first order and critical wetting lines are described by the

unique equation

$$\frac{\sqrt{2}}{\xi_3/\xi} = \sqrt{K-1}. \quad (32)$$

The wetting phase diagram for the complete symmetric system is plotted in Fig. 4. The phase boundary (32) is shown by the blue line. The wetting phase transition is of first order.

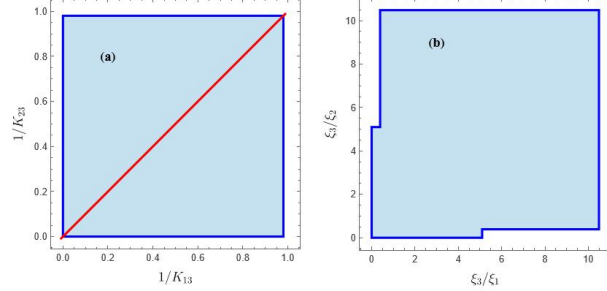


Figure 5: The location of degenerate points in (a) $(1/K_{13}, 1/K_{23})$ -plane and (b) $(\xi_3/\xi_1, \xi_3/\xi_2)$ -plane

3.2. Loci of degenerate points

As discussed in the previous subsection, the nucleation, first-order, and critical wetting lines intersect at degenerate points in the wetting phase diagram. We now examine the loci of these degenerate points in the phase space of the relevant parameters.

In the plane of the relative coupling constants, Eqs. (21) at $\mu_3/\bar{\mu}_3 = 1$, (25) and (28) have two solutions

$$\beta_{13} = \beta_{23} = \frac{1}{\sqrt{2}} \left(\frac{1}{\xi_3/\xi_1} + \frac{1}{\xi_3/\xi_2} \right), \quad (33)$$

and

$$\begin{aligned} \beta_{13} &= \frac{\sqrt{2}}{\xi_3/\xi_1}, \\ \beta_{23} &= \frac{\sqrt{2}}{\xi_3/\xi_2}. \end{aligned} \quad (34)$$

Accordingly, two degenerate points appear in the (K_{13}, K_{23}) -plane. Several remarks follow from (33) and (34):

- The degenerate point associated with Eq. (33) always lies on the bisector of the first quadrant in the $(1/K_{13}, 1/K_{23})$ -plane; its locus corresponds to the red line in Fig. 5(a).

- When the healing-length ratios vary, the degenerate point in Eq. (34) may occupy any point in the region bounded by the blue lines in Fig. 5(a). This point lies on the straight locus ξ_3/ξ_1 or ξ_3/ξ_2 , this point lies on the

straight locus

$$K_{23} = \frac{1 + 2(\xi_2/\xi_3)^2}{1 + 2(\xi_1/\xi_3)^2} K_{13}, \quad (35)$$

indicating that it varies linearly with K_{13} .

- In the symmetric case $\xi_3/\xi_1 = \xi_3/\xi_2$, the two degenerate points coincide.

Alternatively, in the plane of healing-length ratios, only a single degenerate point arises

$$\begin{cases} \frac{\xi_3}{\xi_1} = \frac{\sqrt{2}}{\beta_{13}}, \\ \frac{\xi_3}{\xi_2} = \frac{\sqrt{2}}{\beta_{23}}. \end{cases}, \quad (36)$$

and this point may lie at any location within the region bounded by the blue line in Fig. 5(b).

4. Conclusions

In this work, we have investigated the wetting phase transition in a dilute ternary Bose–Einstein condensate (BEC). Motivated by experimental feasibility, we focused on scenarios in which the intraspecies atomic interactions are tunable, while the interspecies interactions are held fixed.

Our main findings are as follows:

- The locus of the degenerate points in plane of the relative coupling constants has been investigated.
- The nucleation phase transition has been analyzed for a specific set of intrinsic atomic parameters, providing insight into the onset of surfactant-mediated interface modification.
- The wetting phase diagram has been constructed in the space of healing length ratios. Remarkably, it is found that only a single degenerate point exists in this parameter space, in contrast to previous results where two such points were observed in the space of interspecies interaction coupling constants.
- The wetting transition is shown to be either of strongly first-order, marked by the discontinuous transition of slope of the interfacial tension $\gamma_{12(3)}$ at transition point, or of critical characterized by the continuity one, depending on the path taken in the phase diagram.

- Loci of degenerate points have been investigated in both $(1/K_{13}, 1/K_{23})$ - and $(\xi_3/\xi_1, \xi_3/\xi_2)$ -planes.

These results contribute to a deeper understanding of interfacial phenomena in multicomponent BECs and provide theoretical guidance for experimental exploration of wetting transitions in ultracold atomic systems.

Acknowledgements

We thank J. O. Indekeu and J. Berx for their discussion in the early stage of this work. This research is funded by Vietnam National Foundation for Science and Technology Development (NAFOSTED) under grant number 103.01-2023.12.

References

- [1] P. G. de Gennes, Wetting: statics and dynamics, *Reviews of Modern Physics* **57** (3) (1985) 827-863. doi:10.1103/revmodphys.57.827.
- [2] D. Bonn, J. Eggers, J. Indekeu, J. Meunier, E. Rolley, Wetting and spreading, *Reviews of Modern Physics* **81** (2) (2009) 739-805. doi:10.1103/revmodphys.81.739.
- [3] Elsevier, 1965, pp. 546-568. doi:10.1016/b978-0-08-010586-4.50078-x.
- [4] J. Indekeu, J. van Leeuwen, Wetting, prewetting and surface transitions in type-i superconductors, *Physica C: Superconductivity* **251** (3-4) (1995) 290-306. doi:10.1016/0921-4534(95)00421-1.
- [5] V. F. Kozhevnikov, M. J. V. Bael, P. K. Sahoo, K. Temst, C. V. Haesendonck, A. Vantomme, J. O. Indekeu, Observation of wetting-like phase transitions in a surface-enhanced type-I superconductor, *New Journal of Physics* **9** (3) (2007) 75-75. doi:10.1088/1367-2630/9/3/075.
- [6] S. Huang, Y. Zhu, J. Qian, Y. Wan, Y. Yin, L. Zhou, P. Diko, V. Kucharova, K. Zmorayova, Y. Kim, X. Yao, Wetting and spreading of Ca-Y-Ba-Cu-O solution on Y_2O_3 and CaSZ crucible in growing $Y_{1-x}Ca_xBa_2Cu_3O_{7-\delta}$ single crystal, *Journal of the American Ceramic Society* **103** (9) (2020) 4859-4866. doi:10.1111/jace.17212.

- [7] K. Hu, X. Wu, Wetting transition in the transverse-field spin $-\frac{1}{2}xy$ model with boundary fields, *Physical Review B* **107** (13) (2023) 134433. doi:10.1103/physrevb.107.134433.
- [8] J. O. Indekeu, B. V. Schaebybroeck, Extraordinary wetting phase diagram for mixtures of Bose-Einstein condensates, *Physical Review Letters* **93** (21) (2004) 210402. doi:10.1103/physrevlett.93.210402.
- [9] B. Van Schaebybroeck, J. O. Indekeu, Critical wetting, firrst-order wetting, and prewetting phase transitions in binary mixtures of Bose-Einstein condensates, *Physical Review A* **91** (1) (2015) 013626. doi:10.1103/physreva.91.013626.
- [10] P. Duy Thanh, N. Van Thu, Static properties of prewetting phase in binary mixtures of Bose-Einstein condensates, *International Journal of Theoretical Physics* **63** (12) (Dec. 2024). doi:10.1007/s10773-024-05863-w.
- [11] J. O. Indekeu, N. Van Thu, J. Berx, Three-component bose-einstein condensates and wetting without walls, *Physical Review A* **111** (4) (2025), 043320. doi:10.1103/physreva.111.043320.
- [12] D. J. McCarron, H. W. Cho, D. L. Jenkin, M. P. Köppinger, S. L. Cornish, Dual-species bose-einstein condensate ofrb87andcs133, *Physical Review A* **84** (1) (2011), 011603. doi:10.1103/physreva.84.011603.
- [13] M. Egorov, B. Opanchuk, P. Drummond, B. V. Hall, P. Hannaford, A. I. Sidorov, Measurement of s -wave scattering lengths in a two-component Bose-Einstein condensate, *Physical Review A* **87** (5) (2013), 053614. doi:10.1103/physreva.87.053614.
- [14] D. M. Bauer, M. Lettner, C. Vo, G. Rempe, S. Dürr, Control of a magnetic Feshbach resonance with laser light, *Nature Physics* **5** (5) (2009), 339-342. doi:10.1038/nphys1232.
- [15] Y. Liu, J. Li, G.-R. Wang, S.-L. Cong, Optical control of magnetic Feshbach resonances in Bose gases, *Physics Letters A* **378** (1-2) (2014), 43-47. doi:10.1016/j.physleta.2013.10.028.
- [16] P. K. Kanjilal, A. Bhattacharyay, Multicomponent states for trapped spin-1 Bose-Einstein condensates in the presence of a

magnetic field, Physical Review A **108** (5) (2023), 053322. doi:10.1103/physreva.108.053322.

- [17] J. O. Indekeu, C.-Y. Lin, N. Van Thu, B. Van Schaeybroeck, T. H. Phat, Static interfacial properties of Bose-Einstein-condensate mixtures, Physical Review A **91** (3) (2015) 033615. doi:10.1103/physreva.91.033615.
- [18] J. S. Rowlinson, B. Widom, Molecular theory of capillarity, Dover Publications, Mineola, New York, 2002.
- [19] S. Inouye, M. R. Andrews, J. Stenger, H.-J. Miesner, D. M. Stamper-Kurn, W. Ketterle, Observation of feshbach resonances in a Bose-Einstein condensate, Nature **392** (6672) (1998) 151-154. doi:10.1038/32354.
- [20] C. A. Stan, M. W. Zwierlein, C. H. Schunck, S. M. F. Raupach, W. Ketterle, Observation of Feshbach resonances between two different atomic species, Physical Review Letters **93** (14) (2004), 143001. doi:10.1103/physrevlett.93.143001.
- [21] C. Chin, R. Grimm, P. Julienne, E. Tiesinga, Feshbach resonances in ultracold gases, Reviews of Modern Physics **82** (2) (2010) 1225-1286. doi:10.1103/revmodphys.82.1225.